ARTICLE

In Situ Reversible Control between Sliding and Pinning for Diverse Liquids under Ultra-Low Voltage

Chao Chen,[†] Zhouchen Huang,[†] Yunlong Jiao,[†] Lu-An Shi,[‡] Yiyuan Zhang,[†] Jiawen Li,*[†] Chuanzong Li,[§] Xiaodong Lv,[§] Sizhu Wu,[§] Yanlei Hu,[†] Wulin Zhu,[†] Dong Wu,*[†] Jiaru Chu,[†] and Lei Jiang[‖]

[†]CAS Key Laboratory of Mechanical Behavior and Design of Materials, Department of Precision Machinery and Precision Instrumentation and [‡]CAS Center for Excellence in Nanoscience, Hefei Science Center of CAS, Department of Chemistry, University of Science and Technology of China, Hefei 230026, China

[§]School of Instrument Science and Optoelectronics Engineering, Hefei University of Technology, Hefei 230009, China

[‖]Key Laboratory of Bio-inspired Materials and Interfacial Science, Technical Institute of Physics and Chemistry, Chinese Academy of Sciences, Beijing 100190, China

S *Supporting Information*

ABSTRACT: Thermally responsive paraffin-infused slippery surfaces have demonstrated intriguing performance in manipulating the behaviors of versatile droplets. However, present methods have been limited to *ex situ* rigid heat sources with a high voltage of 220 V or certain specific photothermal materials, which greatly hinders its practical applications. To solve this problem, an intelligent droplet motion control actuator (DMCA) composed of paraffin wax, hydrophobic micropillar-arrayed ZnO film, and a flexible transparent silver nanowire heater (SNWH) is reported in this work. Due to the good portability of DMCA, *in situ* switchable wettability for several liquid droplets with different surface tensions can be achieved by simply loading and unloading Joule heat at an ultra-low voltage (12 V). The relationship among sliding velocity and droplet volume and inclined angles was quantitatively investigated. By virtue of the flexible and mechanical endurance, this smart DMCA is dramatically functional for droplet motion manipulation (*e.g.*, reversible control between sliding and pinning) on complex 3D surfaces. Significantly, an impressive self-healing ability within 22 s is also demonstrated through the *in situ* application of Joule heat on the scratched DMCA, which renders its practical usability in various harsh conditions. This work provides insights for designing intelligent, flexible, and portable actuators dealing with the challenges of smart temperature-responsive surfaces.

KEYWORDS: *paraffin-infused slippery surface, flexible silver nanowire heater, droplet motion control actuator, in situ reversible wettability, self-healing*
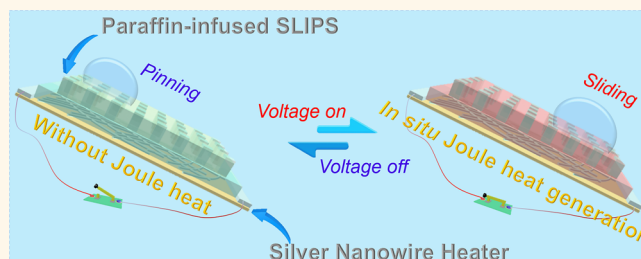
In the past decade, smart surfaces with reversible wettability have aroused enormous interest because of their great potential in both scientific investigations and industrial applications, including droplet-based microfluidics,[1] "no-loss" droplet transportation,[2,3] oil−water separation,[4,5] cell adhesion,[6,7] biotechnology,[8,9] and anti-icing.[10−12] Such switchable wettability could be readily realized by virtue of selectively applying an external stimulus such as photoirradiation,[13−16] temperature,[17−19] an electrical field,[20−23] pH,[24−26] mechanical strain,[27−31] or a magnetic field.[32−42] Typically, Cao et al. developed a photoresponsive organogel surface (POS) composed of Fe₃O₄, polydimethylsiloxane (PDMS), and lubricant silicone oil.[16] Though the switchable wettabilty for diverse liquid droplets has been achieved, this method is only

applicable to special materials but not widely adaptive for others. Banuprasad *et al.* reported a temperature-responsive poly (*N*-isopropylacrylamide) (PNIPAAm) grafted structured hydrophobic PDMS surface for droplet manipulation, which is dependent on the wettability gradient induced by two *ex situ* asymmetric hot plates.[19] Taking advantage of the cooperation by the gradient-structured polystyrene surface and electric field, Tian et al. had realized the continuously driving underwater oil droplets with control of directional motion.[23]
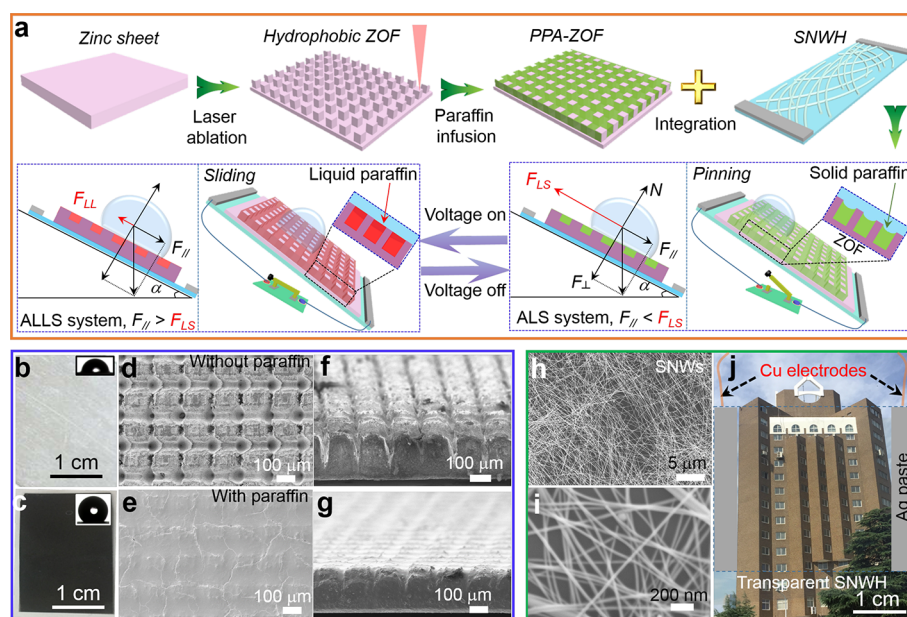
Figure 1. Fabrication of smart DMCA by combining PPA-ZOF with transparent SNWHs. (a) Strategy for preparing smart DMCA including manufacturing hydrophobic micropillar-arrayed ZOF using femtosecond laser ablation, infusing paraffin into micropillar-arrayed ZOF by successive spin-coating, thermal evaporation and condensation processes, and integrating the resultant PPA-ZOF with a flexible SNWH. By virtue of this smart DMCA, the liquid droplet could achieve reversible pinning and sliding at the absence or existence of Joule heat for dynamic control between the frictional ALS and lubricant ALLS system. Digital pictures for zinc sheet (b) before and (c) after being subjected to the femtosecond laser ablation; the insets are the corresponding wettability measurements. SEM images (top view) for micropillar-arrayed ZOF (d) without and (e) with paraffin. The corresponding sectional-view SEM images for micropillar-arrayed ZOF (f) without and (g) with paraffin. SEM images for characterizing the (h) length and (i) diameter of the as-prepared SNWs. (j) Digital picture for an ultratransparent SNWH.

This device is not portable but energy-consuming. Tian et al. utilized a magnetic fluid (MF) infused ZnO nanoarray to steer liquid droplets with controllable and fast-response properties. Though the advanced performance had been achieved by MF, its inherent fluidity and volatility may decrease the longevity of resultant system. Significantly, most of these smart surfaces would inevitably suffer from mechanical abrasion and phasical dmage during use, which may cause a gradual loss of surface wettability and may seriously shorten their operating life. Fortunately, inspired by *Nepenthes* pitcher plants, Aizenberg and co-workers developed the first paradigm of rapidly self-healing, slippery lubricant-infused porous surfaces (SLIPSs).[31] The SLIPSs demonstrate state-of-the-art properties in many respects, including repelling arbitrary simple and complex liquids with suitable lubricants, maintaining low-contact-angle hysteresis and rapidly self-healing after physical damage. Usually, lubricants used in SLIPSs are ionic liquids, silicone oil, low-surface-energy per-fluoropolyethers, or other per-fluorinated liquids that are expensive, volatile, toxic, and harmful to the environment.[43−48]

As the alternative, thermally responsive switching based on paraffin-infused slippery surfaces (PISS) have attracted increasing attentions on account of its ecofriendly, conven-ience, cost-saving, nontoxic, nonvolatility, and good bio-compatibility. For instance, Yao et al. first realized the dynamic control of trapping and sliding for water droplets on *n*-paraffin-swollen organogel by thermally activating the transition between the air/water/solid (ALS) system and air/water/liquid-paraffin/organogel (ALLS) system.[49] Inspired by this classical method, Shiratori and co-workers developed an innovative paraffin-infused porous microstructure utilizing layer-by-layer self-assembly of chitin nanofibers and poly-

(acrylic acid). By controlling the served temperature, this system was capable of endowing the water droplet with switchable wettability and dynamically tunable transmittance simultaneously.[50] Wang et al. presented a novel paraffin-infused porous graphene film (PIPGF) with programmable wettability. When exposed to near-infrared light irradiation, the unmasked pathways of PIPGF allowed the water droplet transition from sticking to slipping because of a lower adhesion of the melt paraffin.[51] Recently, Wang *et al.* reported an anisotropic slippery surface composed of paraffin and polystyrene film, which had been successfully applied in unidirectional control for several liquid droplets with different surface tensions.[52] Although these explorations had extensively advanced the development of smart control for liquid droplets by virtue of thermally responsive paraffin. However, several severe disadvantages have to be considered. (1) To date, switchable wettability is always controlled by an *ex situ* rigid heat-source such a hot-plate or air oven with a relatively energy-consuming voltage of 220 V.[39,40,42] (2) Controlling the droplet motion has been limited to a planar slippery surface, which hinders its practical application in a complex terrain.[39−42] (3) Near-infrared light irradiation is only functional for photothermal materials such as graphene and Fe_3O_4, whereas it is not widely adaptive for various materials.[41]

In this work, we report a Joule-heated droplet motion control actuator (DMCA) by incorporation of flexible silver nanowire heater (SNWH) and paraffin-infused micropillar-arrayed zinc oxide film (PPA-ZOF). Taking the advantage of its good portability, *in situ* switchable wettability for several liquid droplets with different surface tensions can be realized by simply loading/unloading an ultra-low voltage of 12 V. The underlying mechanism is that when direct current (DC)
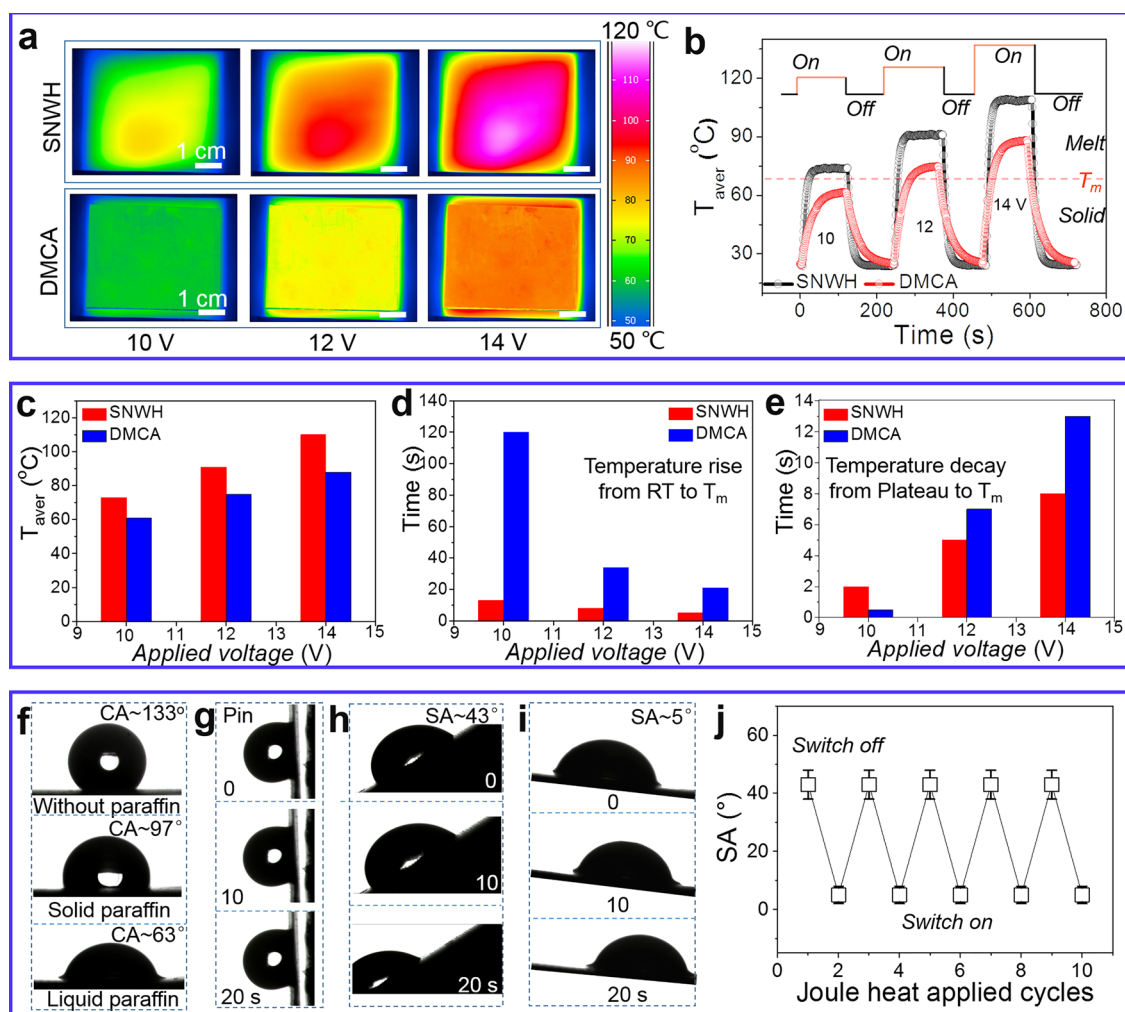
Figure 2. *In situ* switchable wettability of Joule-heated DMCA. (a) Thermal IR images and (b) temperature−time curves for SNWH and DMCA with the applied voltage of 10, 12, and 14 V, respectively. (c) Temperature plateau variation as a function of the applied voltage for SNWH and DMCA. Time required for SNWH and DMCA (d) rising from the room temperature (RT) to 64 °C (melt point of paraffin, T_M) and (e) decreasing from T_M to RT, respectively. (f) WCA measurements for micropillar-arrayed ZOF without paraffin with solid infused paraffin and with Joule-heated lubricant paraffin, respectively. SA measurements for micropillar-arrayed ZOF (g) without paraffin, (h) with solid paraffin, and (i) with Joule-heated lubricant paraffin. (j) Stability test for the smart DMCA by *in situ* loading and discharging Joule heat.

voltage was applied, the generated Joule heat elevated the temperature above the melting point of paraffin within 40 s to turn an adhesive ALS system to a lubricant ALLS one. Once the voltage was switched off, the melt paraffin would rapidly solidify to a frictional ALS system within 4 s through the heat transfer and thermal-radiation processes. This electric-induced-heating electronic device can be suitable for a variety of materials, which is crucial for broad applications. Additionally, owing to its outstanding flexibility and mechanical endurance, this smart DMCA is dramatically functional for *in situ* manipulating the droplet motion on complex 3D surfaces. Significantly, the intelligent DMCA can rapidly self-heal from physical damage by virtue of the capillary effect within 22 s under the assistance of *in situ* Joule heating. This work gives insights for dealing with the challenges of thermally responsive smart surfaces.

RESULTS AND DISCUSSION

Facile Fabrication of Smart DMCA by Combining PPA-ZOF with Flexible SNWH. The desirable DMCA is composed of three crucial components: (1) hydrophobic

flexible porous skeleton (HFPS); (2) temperature-responsive phase-change material (TAPCM); and (3) a portable heater with good flexibility. Accordingly, its fabricating strategy contains femtosecond laser ablation, paraffin infusion, and flexible SNWH integration (Figure 1a).

Therein, HFPS is of great importance for droplet motion control because it provides a giant capillary force to block the lubricant from contaminating the targeted droplets. More importantly, HFPS protects an impressively stable ALLS system from the intrusion of the objective droplets, which is more favorable for dynamic control of droplet motion in comparison with a hydrophilic porous substrate. Accordingly, femtosecond laser microfabrication was employed to manufacture hydrophobic porous structures, which is well-known as a versatile technique for controlling the surface wettability of diverse materials.[53−55] By virtue of a scan-cross mode, the flexible metallic zinc sheet could be readily ablated to an atrous microstructured ZOF with high reflectance (Figures 1b,c and S1). The microstructured ZOF with the typical water contact angle (WCA) of 133 ± 5° exhibited a stable hydrophobic property comparing to the original zinc sheet of 40 ± 4°.

Scanning electron microscopy (SEM) images in parts d and f show that this ZOF was patterned by the ultrauniform micropillar arrays with an interval of ∼50 μm, where the length, width, and height for a single pillar was approximately measured as 100, 100, and 220 μm, respectively. Conducting a further topography investigation by SEM, we found a myriad of tapered wells (TWs) and oblong grooves (OGs) participated in the pillar-arrayed ZOF (Figure S2). These tertiary micro- and nanostructure including pillars, TWs, and OGs are made to be conducive to providing a tremendous capillary force for the lubricant infusion, storage, and blockage. Compared to typical chemical methods, we currently take advantage of one-step femtosecond laser vertical scanning with high fabrication efficiency and accuracy to harvest a desirable hydrophobic platform, which is comparatively more tunable, facile, efficient, and eco-friendly.[49−51] More importantly, the hydropholized micropillar-arrayed ZOF by femtosecond laser presented an outstanding stability as long as 2 months (Figure S3).

In a secondary stage, the typical TAPCM of paraffin with a melting point (T_M) of 64 °C was selected as the lubricant on account of its unique advantages of fast temperature-response, lack of toxicity, low volatility, and cost savings. Herein, paraffin solution (0.1 g/mL, in dichloromethane) could be successfully infused into the as-prepared ZOF utilizing successive spin-coating, thermal evaporation, and condensation. Although numerous wrinkles had been introduced during a solidification process, the infused paraffin was capable of covering the pillar-arrayed ZOF by virtue of the capillary force, which had been verified by a combination of the top and sectional view of PPA-ZOF (Figure 1e,g). By comparing SEM images of micropillar-arrayed ZOF before and after being infused by paraffin, we could estimate the typical thickness of this paraffin layer as 160 μm.

Silver nanowires (SNWs) have attracted extensive research interest because of its potential applications in optoelectronic device and flexible heaters.[56,57,61] In this regard, the polyol method was employed to synthesize high-quality SNWs with an average diameter of 20.7 (±2.8) nm and an average length of 20.0 (±6.5) μm (Figures 1h,i and S4). Thereafter, utilizing an optimized rheology-modified SNW ink (1 mg/mL), the transparent conductive film (TCF) with an average sheet resistance of 88.6 ± 8.1 Ω/sq was fabricated by one-step roll-to-roll method (Figure S5). Subsequently, an ultraflexible SNWH with a high transmittance could be readily harvested through the introduction of a pair of symmetric copper-wire electrodes (Figure 1j). SNWH, having the advantage of faster response to the same electrical stimuli (applied voltage: 12 V) than that of a commercial heater (Com-heater), was demonstrated (Figure S6). Therein, the time spent for SNWH rising from RT to a targeted 64° (melting point of paraffin, T_M) was detected in 8 s compared to that for a Com-heater, 18 s, while the decay time for the former is 5 s in comparison to that for the later, 71 s (Figure S7). Notably, SNWH performance in this work is far more superior or comparable to other previous heaters due to its excellent thermal conductivity and high electric conductivity (Figure S8). The intelligent DMCA could be constructed after an integration of the flexible SNWH and PPA-ZOF by Kapoton.

By the *in situ* application of an ultra-low voltage on DMCA, the solid paraffin would melt, exhibit a heat-expansion phenomenon, and flatten to liquid paraffin when the original frictional resistance between solid paraffin and liquid droplet (f_{LS}) sharply decreased to a frictional resistance derived from liquid paraffin and liquid droplet (f_{LL}). Therein, the liquid droplet achieved the motion from pinning to sliding on DMCA. Thereafter, the liquid droplet would brake on DMCA once the voltage was discharged because the hot paraffin tended to present cold shrinkage, leading to the generation of multiple wrinkles in solid paraffin. As a result, using this smart DMCA, we could control the droplet motion between pinning and sliding by loading or discharging voltage for dynamic control between the frictional ALS and the lubricant ALLS system.

***In Situ* Switchable Wettability of Joule-Heated DMCA.** Thermal infrared imager was carried out for investigating the electric-induced-heating performance for SNWH and DMCA. Once the DC voltage was applied, the homogeneous Joule heat generated across the SNW network had been *in situ* transferred from SNWH in sequence toward the surface paraffin to elevate the temperature of DMCA (Figures 2a and S9). The larger the applied voltage, the more the generated Joule heat. Seen from the temperature−time curves in Figure 2b, the temperature plateaus for SNWH with the served voltages of 10, 12, and 14 V were achieved within 30 s, whereas it was not horizontal for 120 s heating time assigned to DMCA. Similarly, temperature decreased to RT for DMCA was more time-consuming in comparison with that for SNWH. The underlying mechanism for this hysteretic phenomenon could be revealed by taking the advantage of the fundamental physics related to thermodynamics. The harvested temperature of DMCA is determined by two processes: (1) inflow and storage of the electrical energy and the (2) outflow and releasing of the energy through heat transfer in sequence from SNWH to Kapton, ZOF, and paraffin. Velocity for temperature rising from RT to the horizontal plateau (T_{max}) and decreasing from T_{max} to RT could be described using a time constant of the transient thermal response (τ) that is equal to $\rho dc/h$.[57] Therein, ρ, d, c, and h represent the mass density, thickness, specific heat capacity, and heat-transfer coefficient, respectively. These parameters for diverse materials could be detected in Table S1. Accordingly, we deduced that a lager τ assigned to DMCA was supposed to be induced by a Kapton with an exaggerated h, which hindered the fast heat transfer and release to achieve the melting and solidification of paraffin. As a result, thermal conductive adhesive tape with lower h could be selected as the substitution of Kapton for its practical usability in a future work, which should be more beneficial for the optimization of DMCA to harvest a faster temperature response. Notably, by *in situ* loading voltages of 10, 12, and 14 V, SNWH and DMCA were capable of achieving the maximum temperature of 73/61, 91/75, and 110/88 °C, respectively (Figure 2c). With regard of paraffin with a lower T_M of 64 °C, the response time corresponding to the melting and solidification processes were obtained as 120/2, 34/7, and 21/13 s (Figure 2d,e), respectively. After a comprehensive assessment, an optimized input of 12 V with the relatively faster temperature response was adopted for droplet motion control.

Water droplets exhibited a hydrophobic wettability on the pillar-arrayed ZOF (WCA ≈ 133°), whereas they tended to wet the PPA-ZOF (WCA ≈ 97°) with a smaller roughness in comparison with the micro- and nanostructured ZOF. Once 12 V voltage was applied, Joule-heated DMCA elevated the temperature above T_M, and then the WCA was further decreased to 63° via the formation of an ALLS hierarchy (Figure 2f). In addition, pillar-arrayed ZOF without paraffin
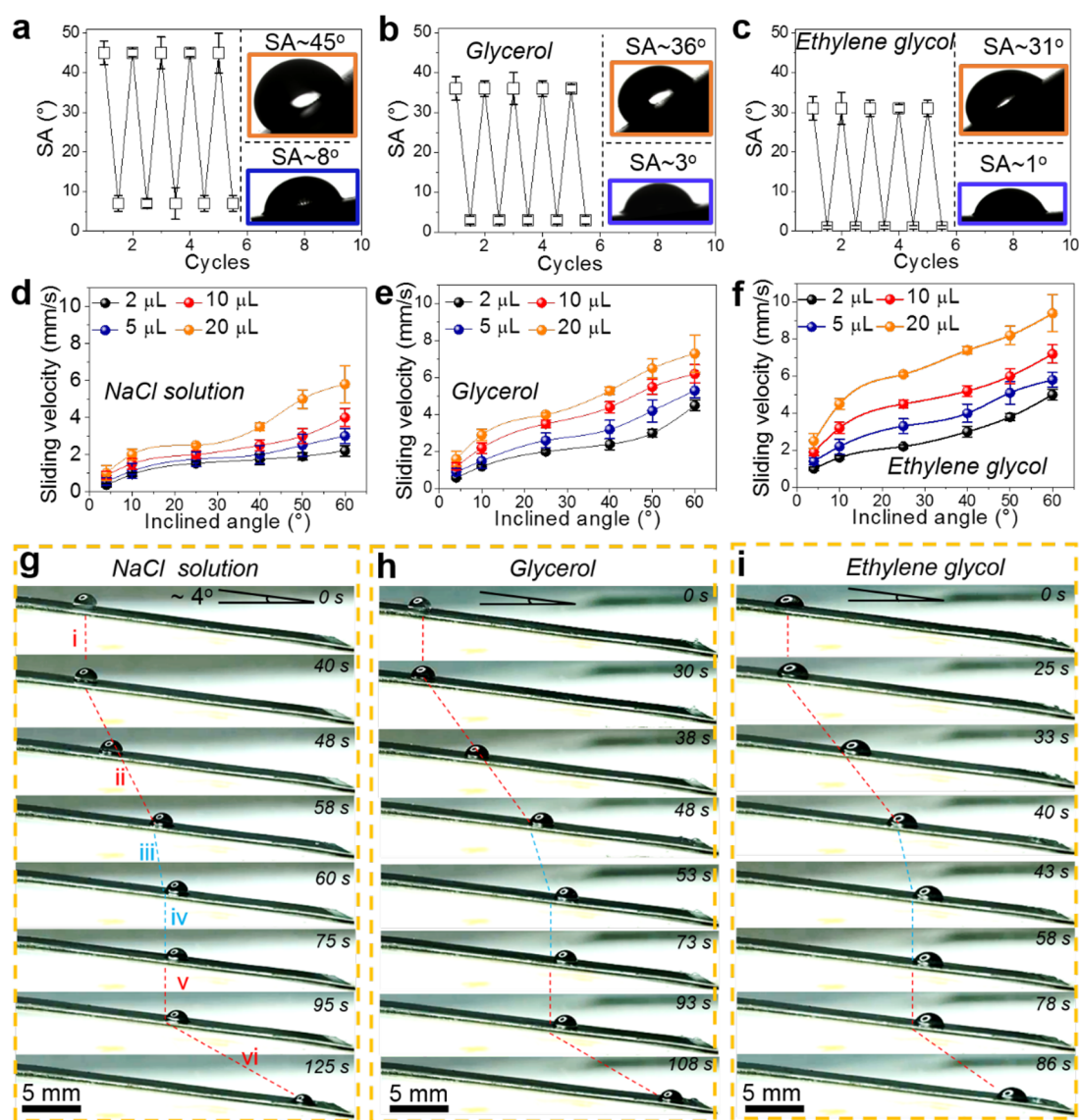
Figure 3. Quantitative investigation of *in situ* motion control for diverse rheological droplets. Cyclic SA measurements for (a) NaCl droplets, (b) glycerol droplets, and (c) EG droplets with the loading and unloading of a voltage of 12 V, respectively. The insets are their corresponding SA characterizations when the voltage (12 V) is switched on or off. Sliding velocity for (d) NaCl droplets, (e) glycerol droplets, and (f) EG droplets with different volumes as the function of the inclined angles. Dynamic motion control (pinning, sliding, pinning, and sliding) for (g) NaCl droplets (~10 μL), (h) glycerol droplets (~10 μL), and (i) EG droplets (~10 μL) by *in situ* pulsed loading and discharging Joule heat (applied voltage: 12 V), respectively. The corresponding motion control by *in situ* Joule-heated DMCA is composed of the following five steps: (i) voltage on, $T < T_M$, droplets pin on DMCA; (ii) voltage on, $T > T_M$, droplets slide on DMCA; (iii) voltage off, $T > T_M$, droplets brake on DMCA within 5 s; (iv) voltage off, $T < T_M$, droplets pin on DMCA; and (v, vi) the same tendency with steps i and ii, respectively.

tended to immobilize the water droplet on account of the ultra-robust adhesive force arising from a Wenzel mode (Figure 2g). In sharp contrast, the paraffin-infused ZOF was able to decrease the surface adhesive force to endow water droplet with a sliding angle (SA) of 43 ± 5° (Figure 2h). Upon further applying an *in situ* electric stimuli, SA of the water droplet on this slippery surface was dramatically decreased to 5 ± 2° (Figure 2i). Moreover, despite *in situ* loading and discharging of Joule heat for 10 cycles, no obvious fluctuation of this switchable wettability for water droplets had been observed (Figure 2j). Significantly, the smart DMCA was capable of maintaining its good electrical and thermal performance even if the heat-tolerance cyclic test had been conducted for 1.5 h (Figure S10). The admirable heat endurance of this intelligent

DMCA was manifested as a highly reliable candidate for practical usability in achieving reversible wettability of liquid droplets. In addition, the corresponding longevity test by *in situ* heating and freezing in tilt DMCA for various cycles had been conducted when we fixed the inclined angle of DMCA at 30°, the heating time at 120 s, the cooling time at 120 s, and the served voltage at 12 V (Figure S11a), respectively. The results indicated that the smart DMCA has excellent morphology stability, good conductivity durability, and outstanding thermal endurance (Figure S11b−d).

Quantitative Investigation of *in Situ* Motion Control for Diverse Rheological Droplets. The fabricated DMCA is expected to control the motion of droplets with diverse rheological properties including saturated NaCl aqueous
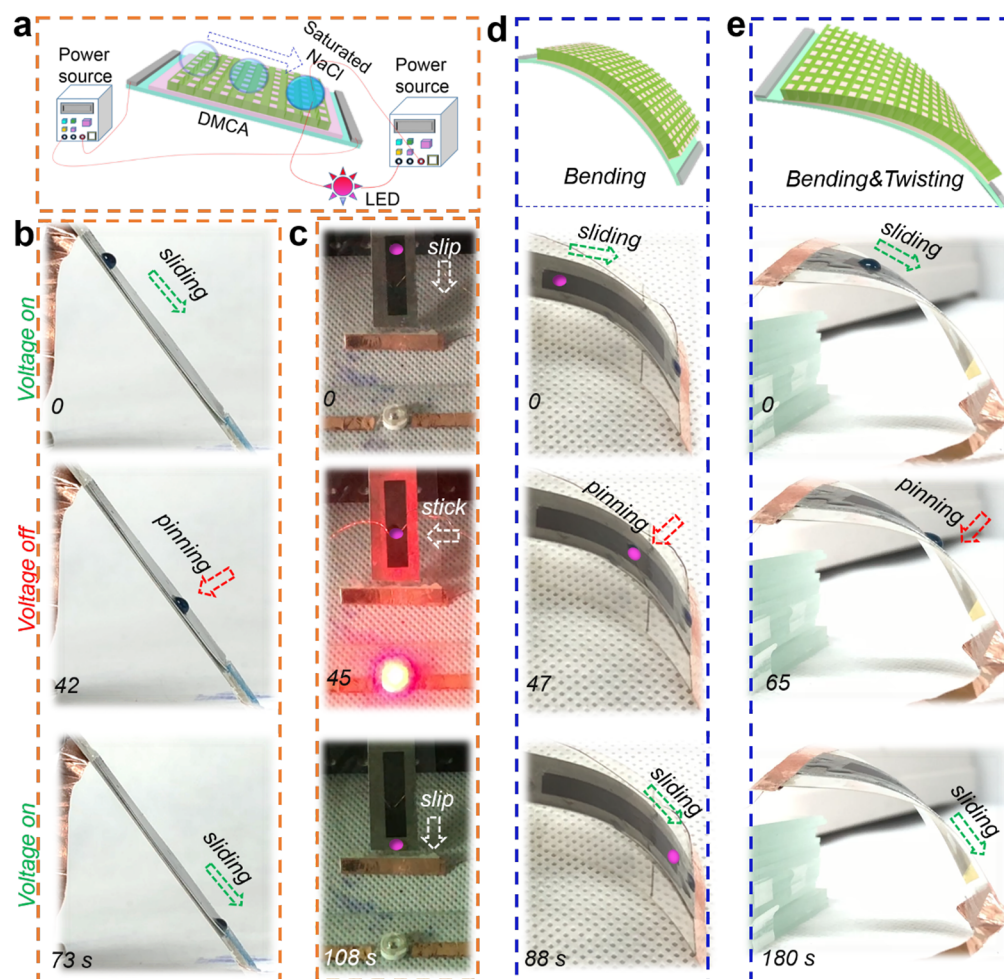
Figure 4. *In situ* reversible droplet control between pinning and sliding on multidimensional surfaces. (a) Home-built electrical circuit incorporated by two power sources, smart DMCA, and saturated NaCl droplet. (b) Sequential pinning–sliding–pinning motion control of water droplet (∼5 µL) on the planar DMCA (inclined angle: ∼47°) by *in situ* loading and unloading the input (applied voltage: 12 V). (c) Manipulating saturated NaCl droplet (∼10 µL) to connect and cut off the electric circuit by *in situ* loading and discharging of Joule heat. Water-droplet motion control by *in situ* loading and unloading of Joule heat on (d) curved and (e) twisted DMCA surfaces.

solution, glycerol, and ethylene glycol (EG) in addition to water droplet. Thus, the cyclic switching on and off of input had been implemented on DMCA to obtain the SAs of three typical liquid droplets. At room temperature, SAs for NaCl solution, glycerol, and EG (5 µL) were measured as 45 ± 3°, 36 ± 2°, and 31 ± 2°, respectively. In contrast, with the *in situ* application of a voltage of 12 V on DMCA, their SAs were successively decreased to 8 ± 3°, 3 ± 1°, and 1° (Figure 3a−c), respectively. Furthermore, sliding velocity as a function of inclined angle measurements for three typical reagents with differential volumes had been also executed in the presence of Joule-heat (Figure 3d−f). The larger the liquid droplet volume, the faster the sliding velocity. In regard of NaCl solution, glycerol and EG with surface tensions of 8.5×10^{-2}, 6.2×10^{-2}, and 4.6×10^{-2} N/m, the sliding velocity had decreased with the increasing surface tension for the same volume of different liquid droplets, signifying that the sliding velocity was inversely proportional to the surface tension.

On the basis of the above investigations, this intelligent actuator was then employed to achieve the *in situ* droplet motion control in a pulsed switch on/switch off operation (Figure S12 and Movies S1−3). Figure 3g−i provides photos for various liquid droplet (10 µL) behavior on the DMCA

surface. (i) For voltage on, $T < T_M$, the liquid droplet tended to stick on the DMCA because the force parallel to the slippery surface derived from gravity $(F_{//})$ was far inferior to the friction in the presence of an ALS system. With the elevation of local temperature, 40 s was required for Joule-heated DMCA rising from RT to a targeted T_M for the sake of ALLS system when NaCl droplet sliding behavior was initiated. In sharp contrast, glycerol and EG droplets with smaller surface tensions had started to slide at 30 and 25 s before the T_M of paraffin was reached, where the surface paraffin should be the construction of the semi-liquid state and the semi-solid state. The smaller the liquid droplet surface tension, the easier the sliding with an identical tilt angle. (ii) For voltage on and $T > T_M$, under the assistance of *in situ* Joule heat, sliding a distance of 5.6, 10.5, and 12.6 mm for NaCl, glycerol and EG droplets needs 18, 18, and 15 s, respectively. It demonstrated that EG with the smallest surface tension presented a fastest sliding velocity under the same inclined angle. (iii) For voltage off and $T > T_M$. After discharging the input, three typical liquid droplets would not be immobilized immediately until sliding a distance of 2.1, 3.5, and 4.2 mm with the corresponding time of 2, 5, and 3 s because of the slow decay of the survived Joule heat in the Kapton. (iv) For voltage off and $T < T_M$, when the
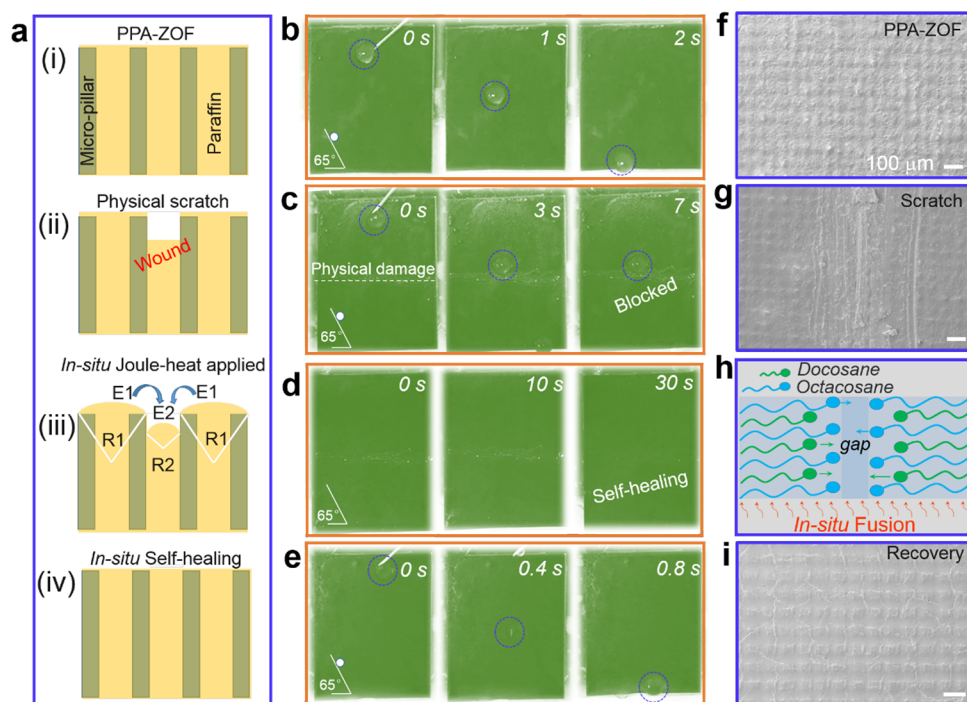
Figure 5. *In situ* self-repairing for Joule-heat-assisted DMCA. (a) Schematic diagram for illustrating the self-repairing process of this smart DMCA depending on the capillary effect. (b) Digital pictures for the undamaged DMCA with a slippery solid surface, allowing the sliding of a typical water droplet (10 μL) within 2 s. (c) Photograph for the scratched DMCA blocking the sliding water droplet. (d) Dynamic pictures for the scratched DMCA achieving the self-repairing within 30 s under the assistance of *in situ* Joule heat. (e) Captured pictures for the self-healed DMCA with a slippery performance comparable or superior to its original surface. SEM pictures for the (f) undamaged, (g) scratched and (i) self-healed DMCA. (h) Schematic diagram representing the dynamic self-repairing process by the chemical fusion of docosane and octacosane in the melted paraffin.

temperature decreased below T_M, one cyclic motion control of stick−slide−stick for three liquid droplets had been successfully achieved. By the same token, another cyclic droplet motion control could be readily realized seen from cases v and vi. To investigate the stability of the paraffin layer, we fixed the DMCA at a constant inclined angle of 30°, the sliding water droplet volume of 50 μL, and the applied voltage of 12 V and allowed the heating and freezing of parraffin for 30, 60, and 90 cycles (Figure S13a), respectively. It is noteworthy that one cycle of the heating and freezing operation corresponds to one 50 μL water droplet sliding over the melt paraffin. The stability of the paraffin layer could be characterized by a profile meter. With the increase of sliding water droplets, the surface roughness increased from 5.5 to 7.2, 10.4, and then 12.7 μm (Figure S13b), respectively. The result revealed that there was indeed severe loss for this paraffin layer after a couple of running, which had been also demonstrated by a localized linescan (Figure S13c,d). According to the lubricant depletion theory proposed by Aizenberg, the dissipative force at the contact line should account for the lubricant sacrifice, which depends nonlinearly on velocity for lubricated surfaces.[62] The interconnected lubricant dynamics results in the growth of the wetting ridge around the droplet, which is the dominant source of lubricant depletion.[63] Interestingly, the DMCA still exhibited an effective dynamic control for water droplet even though it had been subjected to droplet running for 90 cycles (Figure S14 and Movie S9). The underlying mechanism should be assigned to a "slippery Wenzel mode".[64] Notably, the sliding angle (SA) for a water droplet on original heated-DMCA was characterized as 4°, in comparison with that on heated DMCA with 90 cycles of running by water droplets,

which was 26°, which demonstrated the dynamic conversion from lubricant-wrapped sliding to Wenzel mode sliding (Figure S15). Therein, the slippery Wenzel state was provided by the surviving paraffin in nanoporous micropillar-arrayed ZOF, which could be observed from a series of enlarged SEM images (Figure S16). The result is consistent with the previous investigations.[64] In conclusion, although some loss for the paraffin layer had resulted in the elevation of SA, the dynamic control for liquid droplet by DMCA is still fuctional in a manner of the Wenzel slippery state.

***In Situ* Reversible Droplet Motion Control between Pinning and Sliding on 2D and 3D Surfaces.** In practical applications such as anti-fogging and anti-icing, this DMCA should be capable of being functional regardless of surfaces with various complex terrains in addition to traditional 2D surfaces. With regard to the water droplet (5 μL) on a planar DMCA, its sequential "stick-slide-stick" behavior could be readily achieved by virtue of an *in situ* pulsed charging and discharging (Figure 4b and Movie S4). Utilizing a home-built electric circuit, lighting and extinguishing LEDs had been realized on this smart DMCA by *in situ* loading and unloading Joule heat (Figure 4a and Movie S5). Once the voltage (12 V) was applied, the saturated NaCl droplet (5 μL) swam downward within 45 s to connect 2 symmetric copper-wire electrodes and lighten the LED when Joule heat was immediately removed for immobilizing NaCl droplet (Figure 4c). Thereafter, temperature stimuli was applied once more for mobilizing NaCl droplet to cut off the circuit. However, the LED was not inclined to extinguish in the presence of Laplace force arising from two symmetric copper-wire electrodes until the complete removal of the residual NaCl droplet. Even

though the planar DMCA was artificially bent or twisted to complex 3D surfaces, this smart DMCA was still able to manipulate the droplet motion, which should be attributed to the good flexibility of SNWH (Figure S17 and Movies S6 and S7). As shown in parts d and e, when Joule heat was applied, water droplets (5 μL) slide over the liquid paraffin for a long distance. Once the input was cut off, the water droplet was capable of braking within 4 s in spite of an ultra-steep terrain. By the *in situ* loading of Joule heat, the water droplet continue to slip downward on the slippery 3D surface (Figure S18).

***In Situ* Joule-Heat-Assisted Self-Healing.** During the practical usage, the smart DMCA was inevitably subjected to an abrasion or scratch leading to the invalidation of its slippery performance. In this regard, DMCA was expected to display an impressive *in situ* self-healing ability. Inspired by the self-healing process of SLIPS relying on the free flow of the lubricant in the porous film,[58,59] the as-prepared solid slippery surface of DMCA also exhibited excellent self-healing properties similar to SLIPS just after the *in situ* loading of Joule heat, which should be attributed to a capillary effect (Figure 5a). As shown in Figure 5b,c when this solid slippery surface was scratched with a glass cutter, a deep damage gap could be detected on the surface that immobilized the water droplet (10 μL) from sliding for a long time. When *in situ* Joule heat was applied, the melting paraffin can rapidly flow toward the wound by the capillary effect within 22 s and form a smooth liquid layer on the surface (Figure 5d and Movie S8). After the *in situ* unloading of Joule heat, liquid paraffin solidified and the surface self-healed completely to allow the passage of a water droplet (10 μL) (Figure 5e). This *in situ* self-healed performance was also demonstrated by SEM images (Figure 5f–i).

CONCLUSIONS

In summary, a hydrophobic micropillar-arrayed ZOF has been manufactured by vertically crossed scanning of femtosecond laser. By successive spin-coating, thermal evaporation, and condensation procedure, paraffin is successfully infused into the as-prepared ZOF by virtue of capillary force. In addition, a flexible, portable, and ultra-uniform SNWH can be readily harvested by an automatic roll-to-roll method. On this basis, a smart DMCA has been fabricated by the integration of PPA-ZOF and SNWH. Thanks to its excellent portability, *in situ* switchable wettability for various liquid droplets with different surface tensions can be achieved by simply loading and discharging an ultra-low-voltage of 12 V, which has been favorably applied in lighting and extinguishing LEDs. The underlying mechanism is that liquid droplet tends toward wetting and slipping on a melted-paraffin-infused slippery surface (ALLS system) in the presence of Joule- heat, whereas it is inclined toward dewetting and sticking on a solidified-paraffin-infused surface (ALS system) at the absence of Joule heat. We also quantitatively studied the relationship among sliding velocity and droplet volume and inclined angles. More importantly, the intelligent DMCA is capable of *in situ* manipulating droplet motion (reversible control between sliding and pinning) on a complex 3D surface, which is attributed to the outstanding mechanical endurance of SNWH. Significantly, the scratched DMCA can *in situ* self-heal in an ultra-short period of 22 s under the assistance of Joule heat, signifying its practical usability in various harsh conditions. Compared with near-infrared light irradiation for photothermal graphene materials reported before, the electricity-induced-

heating electronic device can be suitable for a variety of materials, which is crucial for broad applications. This work provides insights for designing intelligent devices for *in situ* droplet motion control and anti-fogging and anti-icing on 2D/3D surfaces.

EXPERIMENTAL SECTION

Materials. High-purity zinc sheet with a thickness of 0.3 mm was purchased from Jiarun Metal Materials Co., Ltd. AgNO$_3$ (99.8%) was obtained from Shanghai Qiangshun Chemical Reagent Co., Ltd. Polyvinylpyrrolidone (PVP, MW of 55 000) and hydroxypropyl methylcellulose (HPMC) were purchased from Sigma-Aldrich. Ethylene glycol (EG), glycerol, dichloromethane, NaCl, NaBr, and acetone were donated from Sinopharm Chemical Reagent Co., Ltd. Sagos 9760 and Sagos 3223 were obtained from Sago Co., Ltd. Paraffin wax was provided by Jinan Dingyi Chemical Co., Ltd. Distilled water (H$_2$O, 1 g cm^{-3} density) served as contact-angle test materials.

Femtosecond Laser Fabrication. The micropillar-arrayed zinc oxide film was manufactured by vertically crossed scanning of femtosecond laser. The laser beam (104 fs, 1 kHz, 800 nm) from a regenerative amplified Ti:sapphire femtosecond laser system (Legend Elite-1K-HE, Coherent) was employed for ablation. During the fabrication process, the laser beam was guided onto the sample *via* a galvanometric scanning system (SCANLAB), which made the laser beam focus and scan along the *x* and *y* coordinate direction. The laser power, scan spacing, and speed were set at 350 mW, 50 μm, and 1 mm/s, respectively. Accordingly, the hydrophobic zinc oxide film could be obtained after applying 50 laser pulse numbers.

Fabrication of Smart DMCA. *Preparation of PPA-ZOF.* A total of 2 g of paraffin was dissolved in 20 mL of dichloromethane by vigorous magnetic stirring for 30 min. Next, the concentrated paraffin solution was infused into the microstructured ZOF by spin-coating with a rotating speed of 100 rpm for 10 s. Thereafter, it was allowed to anneal at a 70 °C oven for 1 min to volatilize the dichloromethane. Finally, PPA-ZOF was obtained after a condensation process at room temperature.

Synthesis of High-Quality SNWs. For synthesis, (A) 0.220 M NaBr, (B) 0.210 M NaCl, and (C) 0.505 M PVP in EG were individually prepared for utilization. Fresh AgNO$_3$ was dissolved in EG in an ice-cold ultrasonic bath (4−8 °C) for 5 min. Subsequently 2.5 mL of A, 5 mL of B, 25 mL of C, and 25 mL of AgNO$_3$ (0.265 M) were successively added to a 100 mL flask placed in an oil bath at room temperature. Vigorous stirring was applied for 30 min, and then the temperature in the flask was elevated to 170 °C in 15 min, where the nitrogen gas with a flux of 150 mL min^{-1} was bubbled through the reaction. Thereafter, the flask was corked, and the reaction was left for 1 h without disturbing. The flask was taken off from the oil bath immediately and transferred to the water for cooling once the reaction was terminated.[60,61]

Formulation of SNW Ink. A total of 16 mg of purified SNWs harvested by a positive-pressure filtration and acetone purification procedure were dissolved in 16 mL of DI water with the assistance of 32 mg of HPMC and a Sago-dispersant (v/v 0.0025%), and a Sago-flatting agent (v/v 0.0025%). Finally, 1 mg mL^{-1} SNW ink could be obtained after the mixture was fixed on a table concentrator and allowed to blend for 1.5 h with a rotating speed of 110 rpm.[61]

Preparation of Flexible SNWH. . An automatic coating machine (BEVS 1811/2) equipped with an OSP-40 scraper was utilized to coat the conductive SNW network on flexible PET substrate, where the coating rate and area were fixed at 100 mm s^{-1} and A4 (21.0 cm × 29.7 cm), respectively. The starting button was pressed after the dropping of 1 mL of SNW ink, and highly conductive SNW films were obtained after a brief annealing process at 60 °C for 5 min. Thereafter, two symmetric copper-wire electrodes could be soldered using patterned oblong silver paste. SNWH could be prepared after annealing at 70 °C for 5 h, which was then integrated to PPA-ZOF through a double-faced adhesive Kapton.

Characterization. The micro- and nanostructures induced by the laser were characterized by using a field-emission scanning electron microscope (JSM-6700F). The contact angles of the water droplet, glycerol, and EG (∼5 μL) in air were measured using a CA100C contact-angle system (Innuo) with the sessile drop method. The average values were obtained by measuring five drops at different locations on the same surface. All of the contact-angle measurements were conducted at 10% humidity and 20 °C. The sheet resistance of SNW films were measured using a four-point probe technique (RST-9, Four-Probe Technology). The surface temperatures of the SNWH and DMCA were measured by a thermal infrared camera (VarioCAMhr head 680, InfraTec).

ASSOCIATED CONTENT

Ⓢ Supporting Information

The Supporting Information is available free of charge on the ACS Publications website at DOI: 10.1021/acsnano.9b01180.

A video showing *in situ* motion control utilizing smart DMCA for NaCl droplets by applying and discharging Joule heat (AVI)

A video showing *in situ* motion control utilizing smart DMCA for glycerol droplets by applying and discharging Joule heat (AVI)

A video showing *in situ* motion control utilizing smart DMCA for ethylene glycol droplets by applying and discharging Joule heat (AVI)

A video showing water droplet motion control between pinning and sliding on the planar DMCA surface by *in situ* applying and discharging Joule heat (AVI)

A video showing the manipulation of NaCl droplets to lighting and extinguishing LEDs by *in situ* loading and unloading of Joule heat (AVI)

A video showing water droplet motion control between pinning and sliding on the curved surface utilizing smart DMCA by *in situ* applying and discharging Joule heat (AVI)

A video showing water droplet motion control between pinning and sliding on the bent and twisted DMCA surface by *in situ* applying and discharging Joule heat (AVI)

A video showing *In-situ* Self-healing of Smart DMCA from the Physical Damage by *In-situ* Loading Joule-heat (AVI)

A video showing Smart DMCA still functional for dynamic control of liquid droplet after being subjected to droplet running for 90 cycles (AVI)

Schematic diagrams, detailed characterized images of the resulted ZOF by SEM, numerical statistic and normal fitting curves, an optical image of transparent silver nanowire film and the statistic of its sheet resistance, wettability stability and thermal stability tests, detailed descriptions of the dynamic control of diverse droplets by utilizing a planar DMCA, comparisons of mechanical endurance, detailed descriptions of the dynamic control of typical water droplets, key parameter comparisons, longevity tests, and characterization and description for smart DMCA (PDF)

AUTHOR INFORMATION

Corresponding Authors

*E-mail: jwl@ustc.edu.cn.
*E-mail: dongwu@ustc.edu.cn.

ORCID

Yunlong Jiao: 0000-0001-7718-7342
Jiawen Li: 0000-0003-3950-6212
Yanlei Hu: 0000-0003-1964-0043
Dong Wu: 0000-0003-0623-1515
Jiaru Chu: 0000-0001-6472-8103
Lei Jiang: 0000-0003-4579-728X

Author Contributions

D.W., J.L., J.C., and L.J. conceived of and designed the experiments. C.C., Z.H., L.S., Y.J., Y.Z., C.L., X.L., S.W., Y.H., and W.Z. performed the experiments. C.C. and Z.H. wrote the manuscript. C.C. and Z.H. contributed equally to this work.

Notes

The authors declare no competing financial interest.

REFERENCES

(1) Seo, J.; Lee, S.-K.; Lee, J.; Seung Lee, J.; Kwon, H.; Cho, S.-W.; Ahn, J.-H.; Lee, T. Path-Programmable Water Droplet Manipulations on an Adhesion Controlled Superhydrophobic Surface. *Sci. Rep.* **2015**, 5 (12326), 1 DOI: 10.1038/srep12326.

(2) Kim, D.; Seo, J.; Shin, S.; Lee, S.; Lee, K.; Cho, H.; Shim, W.; Lee, H.-B.-R.; Lee, T. Reversible Liquid Adhesion Switching of Superamphiphobic Pd-Decorated Ag Dendrites *via* Gas-Induced Structural Changes. *Chem. Mater.* **2015**, 27, 4964−4971.

(3) Wang, Z.; Yuan, L.; Wang, L.; Wu, T. Stretchable Super-lyophobic Surfaces for Nearly-Lossless Droplet Transfer. *Sens. Actuators, B* **2017**, 244, 649−654.

(4) Cheng, Z.; Wang, J.; Lai, H.; Du, Y.; Hou, R.; Li, C.; Zhang, N.; Sun, K. pH-Controllable On-Demand Oil/Water Separation on the Switchable Superhydrophobic/Superhydrophilic and Underwater Low-Adhesive Superoleophobic Copper Mesh Film. *Langmuir* **2015**, 31, 1393−1399.

(5) Zheng, X.; Guo, Z.; Tian, D.; Zhang, X.; Jiang, L. Electric Field Induced Switchable Wettability to Water on the Polyaniline Membrane and Oil/Water Separation. *Adv. Mater. Interfaces* **2016**, 3 (18), 1600461.

(6) Ishizaki, T.; Saito, N.; Takai, O. Correlation of Cell Adhesive Behaviors on Superhydrophobic, Superhydrophilic, and Micro-patterned Superhydrophobic/Superhydrophilic Surfaces to Their Surface Chemistry. *Langmuir* **2010**, 26, 8147−8154.

(7) Lourenco, B. N.; Marchioli, G.; Song, W.; Reis, R. L.; Van Blitterswijk, C. A.; Karperien, M.; Van Apeldoorn, A.; Mano, J. F. Wettability Influences Cell Behavior on Superhydrophobic Surfaces with Different Topographies. *Biointerphases* **2012**, 7 (46), 46.

(8) Ista, L. K.; Mendez, S.; Lopez, G. P. Attachment and Detachment of Bacteria on Surfaces with Tunable and Switchable Wettability. *Biofouling* **2010**, 26, 111−118.

(9) Wang, L.; Wang, H.; Yuan, L.; Yang, W.; Wu, Z.; Chen, H. Step Wise Control of Protein Adsorption and Bacterial Attachment on a Nanowire Array Surface: Tuning Surface Wettability by Salt Concentration. *J. Mater. Chem.* **2011**, 21, 13920−13925.

(10) Kim, P.; Wong, T. S.; Alvarenga, J.; Kreder, M. J.; Adorno-Martinez, W. E.; Aizenberg, J. Liquid-Infused Nanostructured

Surfaces with Extreme Anti-Ice and Anti-Frost Performance. *ACS Nano* **2012**, *6*, 6569−6577.

(11) Subramanyam, S. B.; Rykaczewski, K.; Varanasi, K. K. Ice Adhesion on Lubricant-Impregnated Textured Surfaces. *Langmuir* **2013**, *29*, 13414−13418.

(12) Song, J.; Lv, Y.; Jiang, L.; Wang, J. Bio-Inspired Strategies for Anti-Icing. *ACS Nano* **2014**, *8*, 3152−3169.

(13) Uyama, A.; Yamazoe, S.; Shigematsu, S.; Morimoto, M.; Yokojima, S.; Mayama, H.; Kojima, Y.; Nakamura, S.; Uchida, K. Reversible Photocontrol of Surface Wettability between Hydrophilic and Superhydrophobic Surfaces on an Asymmetric Diarylethene Solid Surface. *Langmuir* **2011**, *27*, 6395−6400.

(14) Pan, S.; Guo, R.; Xu, W. Photoresponsive Superhydrophobic Surfaces for Effective Wetting Control. *Soft Matter* **2014**, *10*, 9187−9192.

(15) Aria, A. I.; Gharib, M. Reversible Tuning of the Wettability of Carbon Nanotube Arrays: The Effect of Ultraviolet/Ozone and Vacuum Pyrolysis Treatments. *Langmuir* **2011**, *27*, 9005−9011.

(16) Gao, C.; Wang, L.; Lin, Y.; Li, J.; Liu, Y.; Li, X.; Feng, S.; Zheng, Y. Droplets Manipulated on Photothermal Organogel Surfaces. *Adv. Funct. Mater.* **2018**, *28*, 1803072.

(17) Sarwate, P.; Chakraborty, A.; Garg, V.; Luo, C. Controllable Strain Recovery of Shape Memory Polystyrene to Achieve Superhydrophobicity with Tunable Adhesion. *J. Micromech. Microeng.* **2014**, *24*, 115006.

(18) Li, C.; Guo, R.; Jiang, X.; Hu, S.; Li, L.; Cao, X.; Yang, H.; Song, Y.; Ma, Y.; Jiang, L. Reversible Switching of Water-Droplet Mobility on a Superhydrophobic Surface Based on a Phase Transition of a Side Chain Liquid-Crystal Polymer. *Adv. Mater.* **2009**, *21*, 4254−4258.

(19) Banuprasad, T.; Vinay, T.; Subash, C.; Varghese, S.; George, S.; Varanakkottu, S. Transport of Water Droplets over a Thermo-Switchable Surface Using Rewritable Wettability Gradient. *ACS Appl. Mater. Interfaces* **2017**, *9*, 28046−28054.

(20) Lahann, J.; Mitragotri, S.; Tran, T.-N.; Kaido, H.; Sundaram, J.; Choi, I. S.; Hoffer, S.; Somorjai, G. A.; Langer, R. A Reversibly Switching Surface. *Science* **2003**, *299*, 371−374.

(21) Krupenkin, T. N.; Taylor, J. A.; Wang, E. N.; Kolodner, P.; Hodes, M.; Salamon, T. R. Reversible Wetting-Dewetting Transitions on Electrically Tunable Superhydrophobic Nanostructured Surfaces. *Langmuir* **2007**, *23*, 9128−9133.

(22) Verplanck, N.; Galopin, E.; Camart, J.-C.; Thomy, V.; Coffinier, Y.; Boukherroub, R. Reversible Electrowetting on Superhydrophobic Silicon Nanowires. *Nano Lett.* **2007**, *7*, 813−817.

(23) Li, Y.; He, L.; Zhang, X.; Zhang, N.; Tian, D. External-Field-Induced Gradient Wetting for Controllable Liquid Transport: From Movement on the Surface to Penetration into the Surface. *Adv. Mater.* **2017**, *29*, 1703802.

(24) Wang, S.; Liu, H.; Liu, D.; Ma, X.; Fang, X.; Jiang, L. Enthalpy Driven Three-State Switching of a Superhydrophilic/Superhydrophobic Surface. *Angew. Chem., Int. Ed.* **2007**, *46*, 3915−3917.

(25) Xu, Z.; Zhao, Y.; Wang, H.; Zhou, H.; Qin, C.; Wang, X.; Lin, T. Fluorine-Free Superhydrophobic Coatings with pH-Induced Wettability Transition for Controllable Oil-Water Separation. *ACS Appl. Mater. Interfaces* **2016**, *8*, 5661−5667.

(26) Li, J.-J.; Zhou, Y.-N.; Luo, Z.-H. Smart Fiber Membrane for pH Induced Oil/Water Separation. *ACS Appl. Mater. Interfaces* **2015**, *7*, 19643−19650.

(27) Lin, P. C.; Vajpayee, S.; Jagota, A.; Hui, C. Y.; Yang, S. Mechanically Tunable Dry Adhesive From Wrinkled Elastomers. *Soft Matter* **2008**, *4*, 1830−1835.

(28) Wu, D.; Wu, S. Z.; Chen, Q. D.; Zhang, Y. L.; Yao, J.; Yao, X.; Niu, L. G.; Wang, J. N.; Jiang, L.; Sun, H. B. Curvature-Driven Reversible *In Situ* Switching Between Pinned and Roll-Down Superhydrophobic States for Water Droplet Transportation. *Adv. Mater.* **2011**, *23*, 545−549.

(29) Goel, P.; Kumar, S.; Sarkar, J.; Singh, J. P. Mechanical Strain Induced Tunable Anisotropic Wetting on Buckled PDMS Silver Nanorods Arrays. *ACS Appl. Mater. Interfaces* **2015**, *7*, 8419−8426.

(30) Park, J. K.; Yang, Z.; Kim, S. Black Silicon/Elastomer Composite Surface with Switchable Wettability and Adhesion between Lotus and Rose Petal Effects by Mechanical Strain. *ACS Appl. Mater. Interfaces* **2017**, *9*, 33333−33340.

(31) Yao, X.; Hu, Y.; Grinthal, A.; Wong, T. S.; Mahadevan, L.; Aizenberg, J. Adaptive Fluid-Infused Porous Films with Tunable Transparency and Wettability. *Nat. Mater.* **2013**, *12* (529), 529.

(32) Cao, M.; Jin, X.; Peng, Y.; Yu, C.; Li, K.; Liu, K.; Jiang, L. Unidirectional Wetting Properties on Multi-Bioinspired Magneto-controllable Slippery Microcilia. *Adv. Mater.* **2017**, *29* (23), 1606869.

(33) Huang, Y.; Stogin, B. B.; Sun, N.; Wang, J.; Yang, S.; Wong, T.-S. A Switchable Cross-Species Liquid Repellent Surface. *Adv. Mater.* **2017**, *29* (8), 1604641.

(34) Hong, X.; Gao, X.; Jiang, L. Application of Superhydrophobic Surface with High Adhesive Force in No Lost Transport of Superparamagnetic Microdroplet. *J. Am. Chem. Soc.* **2007**, *129*, 1478−1479.

(35) Cheng, Z.; Feng, L.; Jiang, L. Tunable Adhesive Super-hydrophobic Surfaces for Superparamagnetic Microdroplets. *Adv. Funct. Mater.* **2008**, *18*, 3219−3225.

(36) Zhou, Q.; Ristenpart, W. D.; Stroeve, P. Magnetically Induced Decrease in Droplet Contact Angle on Nanostructured Surfaces. *Langmuir* **2011**, *27*, 11747−11751.

(37) Grigoryev, A.; Tokarev, I.; Kornev, K. G.; Luzinov, I.; Minko, S. Superomniphobic Magnetic Microtextures with Remote Wetting Control. *J. Am. Chem. Soc.* **2012**, *134*, 12916−12919.

(38) Drotlef, D.; Blumler, P.; Del Campo, A. Magnetically Actuated Patterns for Bioinspired Reversible Adhesion (Dry and Wet). *Adv. Mater.* **2014**, *26*, 775−779.

(39) Drotlef, D.; Blumler, P.; Papadopoulos, P.; Del Campo, A. Magnetically Actuated Micropatterns for Switchable Wettability. *ACS Appl. Mater. Interfaces* **2014**, *6*, 8702−8707.

(40) Lee, S.; Yim, C. Y.; Kim, Y.; Jeon, S. Magnetorheological Elastomer Films with Tunable Wetting and Adhesion Properties. *ACS Appl. Mater. Interfaces* **2015**, *7*, 19853−19856.

(41) Hou, G.; Cao, M.; Yu, C.; Zheng, S.; Wang, D.; Zhu, Z.; Miao, W.; Tian, Y.; Jiang, L. Foolproof Method for Fast and Reversible Switching of Water Droplet Adhesion by Magnetic Gradients. *ACS Appl. Mater. Interfaces* **2017**, *9*, 23238−23245.

(42) Tian, D.; He, L.; Zhang, N.; Dou, Y.; Jiang, L.; Zheng, X.; Zhang, X.; Guo, Z. Electric Field and Gradient Microstructure for Cooperative Driving of Directional Motion of Underwater Oil Droplets. *Adv. Funct. Mater.* **2016**, *26*, 7986−7992.

(43) Sunny, S.; Vogel, N.; Howell, C.; Vu, T.; Aizenberg, J. Lubricant-Infused Nanoparticulate Coatings Assembled by Layer-by-Layer Deposition. *Adv. Funct. Mater.* **2014**, *24*, 6658−6667.

(44) Wooh, S.; Vollmer, D. Silicone Brushes: Omniphobic Surfaces with Low Sliding Angles. *Angew. Chem., Int. Ed.* **2016**, *55*, 6822−6824.

(45) Zhang, J.; Wang, A.; Seeger, S. Nepenthes Pitcher Inspired Anti-Wetting Silicone Nanofilaments Coatings: Preparation, Unique Anti-Wetting and Self-Cleaning Behaviors. *Adv. Funct. Mater.* **2014**, *24*, 1074−1080.

(46) Guo, T.; Che, P.; Heng, L.; Fan, L.; Jiang, L. Anisotropic Slippery Surfaces: Electric-Driven Smart Control of a Drop's Slide. *Adv. Mater.* **2016**, *28*, 6999−7007.

(47) He, M.; Zhou, X.; Zeng, X.; Cui, D.; Zhang, Q.; Chen, J.; Li, H.; Wang, J.; Cao, Z.; Song, Y.; Jiang, L. Hierarchically Structured Porous Aluminum Surfaces for High-Efficient Removal of Condensed Water. *Soft Matter* **2012**, *8*, 6680−6683.

(48) Che, P.; Heng, L.; Jiang, L. Lubricant-Infused Anisotropic Porous Surface Design of Reduced Graphene Oxide Toward Electrically Driven Smart Control of Conductive Droplets' Motion. *Adv. Funct. Mater.* **2017**, *27*, 1606199.

(49) Yao, X.; Ju, J.; Yang, S.; Wang, J.; Jiang, L. Temperature-Driven Switching of Water Adhesion on Organogel Surface. *Adv. Mater.* **2014**, *26*, 1895−1900.

(50) Manabe, K.; Matsubayashi, T.; Tenjimbayashi, M.; Moriya, T.; Tsuge, Y.; Kyung, K. H.; Shiratori, S. Controllable Broadband Optical Transparency and Wettability Switching of Temperature-Activated

Solid/Liquid-Infused Nanofibrous Membranes. *ACS Nano* **2016**, *10*, 9387−9396.

(51) Wang, J.; Gao, W.; Zhang, H.; Zou, M.; Chen, Y.; Zhao, Y. Programmable Wettability on Photocontrolled Graphene Film. *Sci. Adv.* **2018**, *4*, 1.

(52) Wang, B. L.; Heng, L.; Jiang, L. Temperature-Responsive Anisotropic Slippery Surface for Smart Control of the Droplet Motion. *ACS Appl. Mater. Interfaces* **2018**, *10*, 7442−7450.

(53) Yong, J.; Chen, F.; Yang, Q.; Zhang, D.; Farooq, U.; Du, G.; Hou, X. Bioinspired Underwater Superoleophobic Surface with Ultralow Oil-Adhesion Achieved by Femtosecond Laser Micro-fabrication. *J. Mater. Chem. A* **2014**, *2*, 8790−8795.

(54) Li, G.; Fan, H.; Ren, F.; Zhou, C.; Zhang, Z.; Xu, B.; Wu, S.; Hu, Y.; Zhu, W.; Li, J.; Zeng, Y.; Li, X.; Chu, J.; Wu, D. Multifunctional Ultrathin Aluminum Foil: Oil/Water Separation and Particle Filtration. *J. Mater. Chem. A* **2016**, *4*, 18832−18840.

(55) Yong, J.; Chen, F.; Yang, Q.; Fang, Y.; Huo, J.; Hou, X. Femtosecond Laser Induced Hierarchical ZnO Superhydrophobic Surfaces with Switchable Wettability. *Chem. Commun.* **2015**, *51*, 9813−9816.

(56) Sorel, S.; Bellet, D.; Coleman, J. N. Relationship Between Material Properties and Transparent Heater Performance for Both Bulk-Like and Percolative Nanostructured Networks. *ACS Nano* **2014**, *8*, 4805−4814.

(57) Ji, S.; He, W.; Wang, K.; Ran, Y.; Ye, C. Thermal Response of Transparent Silver Nanowire/PEDOT: PSS Film Heaters. *Small* **2014**, *10*, 4951−4960.

(58) Wong, T. S.; Kang, S. H.; Tang, S. K.; Smythe, E. J.; Hatton, B. D.; Grinthal, A.; Aizenberg, J. Bioinspired Self-Repairing Slippery Surfaces with Pressure-Stable Omniphobicity. *Nature* **2011**, *477*, 443−447.

(59) Vogel, N.; Belisle, R. A.; Hatton, B.; Wong, T. S.; Aizenberg, J. Transparency and Damage Tolerance of Patternable Omniphobic Lubricated Surfaces Based on Inverse Colloidal Monolayers. *Nat. Commun.* **2013**, *4* (2176), 1 DOI: 10.1038/ncomms3176.

(60) Jia, D.; Zhao, Y.; Wei, W.; Chen, C.; Lei, G.; Wan, M.; Tao, J.; Li, S.; Ji, S.; Ye, C. Synthesis of Very Thin Ag Nanowires with Fewer Particles by Suppressing Secondary Seeding. *CrystEngComm* **2017**, *19*, 148−153.

(61) Chen, C.; Zhao, Y.; Wei, W.; Tao, J.; Lei, G.; Jia, D.; Wan, M.; Li, S.; Ji, S.; Ye, C. Fabrication of Silver Nanowire Transparent Conductive Films with an Ultra-Low Haze and Ultra-High Uniformity and Their Application in Transparent Electronics. *J. Mater. Chem. C* **2017**, *5*, 2240−2246.

(62) Daniel, D.; Timonen, J.; Li, R.; Velling, S.; Kreder, M.; Tetreault, A.; Aizenberg, J. Origins of Extreme Liquid Repellency on Structured, Flat, and Lubricated Hydrophobic Surfaces. *Phys. Rev. Lett.* **2018**, *120*, 244503.

(63) Kreder, M.; Daniel, D.; Tetreault, A.; Cao, Z.; Lemaire, B.; Timonen, J.; Aizenberg, J. Film Dynamics and Lubricant Depletion by Droplets Moving on Lubricated Surfaces. *Phys. Rev. X* **2018**, *8*, 031053.

(64) Dai, X.; Stogin, B.; Yang, S.; Wong, T. Slippery Wenzel State. *ACS Nano* **2015**, *9*, 9260−9267.